

Research article

How is cut and chip wear influenced by the variation of the cross-link density within the conventional vulcanization system of natural rubber?

Marek Pöschl¹, Radek Stoček^{1*}, Petr Zádrapa¹, Martin Stěnička¹, Gert Heinrich^{2,3}

¹Centre of Polymer Systems, Tomas Bata University in Zlín, tř. Tomáše Bati 5678, 76001 Zlín, Czech Republic

²Institute of Textile Machinery and High Performance Material Technology, Technical University in Dresden, Hohe Str. 6, 01069 Dresden, Germany

³Leibniz Institute of Polymer Research, Hohe Str. 6, 01069 Dresden, Germany

Received 10 July 2024; accepted in revised form 3 September 2024

Abstract. This paper extends previous studies by the authors that aimed to describe the effect of apparent cross-link density (*CLD*) of the rubber polymer networks on the fracture mechanism caused by cut and chip (*CC*) wear of natural rubber (*NR*), demonstrating the positive effect of conventional vulcanization (*CV*). This work is focused on the determination of the effect of *CLD* while keeping constant the accelerator-to-sulfur ratio $A/S = 0.2$, typical for *CV* systems. For this ratio, different sulfur quantities were chosen, and the concentration of the accelerator *N*-tert-butyl-benzothiazole sulphonamide (*TBBS*) was calculated to achieve *CLDs* in a range from 35 to 524 $\mu\text{mol}\cdot\text{cm}^{-3}$.

Standard analyses such as tensile tests, hardness, rebound resilience and DIN abrasion were performed. From these analyses, the optimum physical properties of the *NR*-based rubber were estimated to be in the *CLD* range of approximately 60 to 160 $\mu\text{mol}\cdot\text{cm}^{-3}$. A *CC* wear analysis was performed with an Instrumented cut and chip analyzer (*ICCA*) and it was found that the highest *CC* wear resistance of the *NR* is in the *CLD* range of 35 to 100 $\mu\text{mol}\cdot\text{cm}^{-3}$. Furthermore, the effect of strain-induced crystallization (*SIC*) of *NR* on *CC* wear and its dependence on the *CLD* region was discussed. For the first time, we determine a *CLD* range for a *CV* system in which the material achieves both optimal mechanical properties and *CC* wear resistance.

Keywords: cut and chip wear; natural rubber; sulfur; accelerator; mechanical properties; apparent cross-link density; strain-induced crystallization; testing

1. Introduction

The use of off-the-road tires (*OTR*), e.g., for agricultural, construction, and forestry machinery, or of conventional truck and car tires in low-traffic areas on very rough concrete or asphalt roads leads to heavy wear and damage to the tread. The same happens with rubber products when used on conveyor belts or rubber tracks. Such wear occurs, for example, when the tire rolls and slides over a sharp surface such as a stone, root, stalk, etc., where high-stress concentrations occur in the tread of the tire at

the tips of the sharp surfaces, which press into the rubber. When this stress exceeds the threshold strength of the applied rubber, a cut will occur. Further rolling of the tire and the associated traction or braking forces on such severe terrain then cause pieces of rubber to detach from the tread. These wear phenomena are well known as cut and chip (*CC*) mechanisms, also termed *CCC*, which stands for cut, chip, and chunk wear field conditions [1, 2].

Generally, tire treads are made from both natural (*NR*) and synthetic rubber (*SR*), and the use of *NR*

*Corresponding author, e-mail: stocек@utb.cz

© BME-PT

has many advantages over SR for heavily loaded tires (e.g., commercial tires). NR is a renewable resource that has high elasticity and tensile strength, as well as low self-heating under cyclic loading [3–5]. Another advantage is its high resistance to crack growth under dynamic cyclic loading. The cause is strain-induced crystallization (SIC) [6], which, combined with the high ultimate strength, gives NR favorable properties for use in applications where very high dynamic loads occur, as is the case with tire treads in difficult terrain. On the other hand, NR has a low resistance to crack initiation compared to synthetic rubber, *i.e.*, it has a low fatigue threshold strength [7, 8]. In effect, this means that even at very low loads, the rubber chains in such rubber will initially break, and thus, cracks appear. Such lower loads occur, *e.g.*, when tires are operated on smooth roads where abrasion due to rubber fatigue predominates, *i.e.*, when the tires slide with lateral slip over road roughness in the nanometer or micrometer range. Thus, NR has very limited resistance to fatigue wear; however, it is highly resistant to CC wear in tires on severe roads. **Figure 1** shows photographs of tires with visible CC wear, and it can be observed that CC wear is the dominant mechanism that caused the damage to both

tires, despite the fact that both tires are used for different purposes. **Figure 1a**, shows a forestry equipment tire used exclusively in a forest environment, whereas **Figure 1b**, shows a multipurpose tire (MPT) operated in various terrains. Their connecting feature is that the treads of both tires contain a high amount of NR, which is specifically resistant to CC wear. So, the question arises as to why CC wear is the predominant mechanism that damages these tires considerably when they are made of NR and should be resistant to CC wear. In practice, various reasons may occur: (i) the tires have been stressed beyond the ultimate strength of the rubber in very difficult terrain, (ii) the compound formulation contains an ingredient that reduces resistance to CC, such as a synthetic rubber or various types of fillers, (iii) the material has been subject to physical aging, or (iv) the selected vulcanization system turned out to be unsuitable, *etc.* The common reason (iv) is the subject of the investigations carried out here.

Vulcanization or curing, or cross-linking leads in the rubber industry to the formation of covalent sulfur bonds between polymer molecules [9]. The choice of a suitable vulcanization system is crucial for achieving optimum rubber resistance to CC wear, as



Figure 1. Photographs of the worn tire treads illustrating the CC wear mechanism: forestry equipment tire (a), and MPT (b).

already described in [10]. Within the previous work, the CC resistance of NR has been studied over the complete range of applicable curing systems, namely conventional (CV), semi-effective (SEV), and effective (EV) by variation of the cross-link density (*CLD*). Finally, it has been found that the CC wear resistance of NR is the highest in the region of action of the CV system. Therefore, this work focuses on the experimental determination of the effect of *CLD* while keeping the accelerator-to-sulfur ratio $A/S = 0.2$, which is exactly typical of a CV curing system, to determine the range of *CLD*, where both the mechanical properties and CC wear resistance are well-balanced and optimal. Therefore, it is necessary to first analyze the curing system in detail.

Sulfur is the most commonly used as a curing agent. The most widely used rubbers are those with ‘high diene content’, e.g., NR, styrene-butadiene rubber (SBR), and butadiene rubber (BR), which are vulcanized with sulfur in the presence of organic accelerators. Accelerated vulcanization of these rubbers using sulfur, together with the vulcanization of other rubbers cured by a closely related technology, accounts for more than 90% of all vulcanizations [11, 12]. Whereas the remaining part creates vulcanizates based on different curing agents such as peroxides, metallic oxide, or bismaleimide [13–16]. In general, the curing system is composed of the activators of vulcanization, accelerators, and curing agents. The activator of sulfur vulcanization is composed of ZnO and stearic acid [11, 15]. The application of activators and accelerators in rubber compounds reduces the curing time from several hours to a few minutes, which is both economically and ecologically primary. The type of concentration of accelerators and sulfur curing agent determines the type of bonds and the *CLD*, whereas the following types of bonds are present: Monosulfide (CSC), disulfide (CS₂C), and polysulfide (C–S_x–C). Based on the quantity of individual types of bonds or their combination, three special types of systems are well-known, which are already mentioned above, and are CV, SEV, and EV systems. These curing systems can be uniquely characterized by the ratio of the amount of accelerator-to-sulfur A/S ratio. CV systems are characterized in the range of A/S from 0.1 to 0.6 and generally generate *CLD* with 95% poly- and disulfide cross-links, and the remaining 5% are monosulfide bonds [17]. The CV systems provide great resistance against fatigue loading but reduced thermal resistance. SEV curing

system obtained A/S ratio in the range from 0.7 to 2.5 and is characterized by 50% poly- and disulfide bonds, whereas the remaining 50% are monosulfide bonds. A SEV curing system composed of approximately the equivalent of the accelerator-to-sulfur ratio, $A/S = 1.0$, will provide vulcanizates with a good compromise between physical properties and resistance to thermo-oxidative aging [18–20]. EV curing systems are those where a low level of sulfur and a correspondingly high level of accelerator or sulfur-less curing are employed in vulcanizates with an $A/S = 2.5$ or more. EV is characterized due to more than 80% of monosulfide bonds. Therefore, an EV system exhibits very high self-heating and limited reversion. On the other hand, CV and SEV systems exhibit significant reversion when exposed to a temperature-time treatment [19–21].

The intensity of the cross-linking generation can be characterized by the *CLD*, whose absolute value increases with increasing A/S ratio. Individual curing systems produce different *CLDs*, the lowest being the CV system, followed by the SEV system, with the highest *CLD* being achieved by the EV system. [22, 23]. The *CLD* plays a crucial role because it directly influences the mechanical behavior of cured rubber, e.g., the modulus and hardness increase monotonically with increasing *CLD*, and the material becomes more elastic with lower hysteresis, which causes a decrease in self-heating and improvement in resistance to thermal aging of such rubbers. [16, 23, 24]. Another phenomenon to consider is the SIC of some rubbers, such as NR and chloroprene rubber (CR). When rubber is stretched, the molecules are arranged in a regular ordered shape in a crystalline structure [25]. The ability to form crystals increases with increasing deformation and exposure time. It has been evaluated experimentally that the onset of SIC in unfilled NR occurs at a tensile strain of ~400%; however, at lower strain values when carbon black (CB) is added as filler [26].

Thus, SIC is the most applied at high deformations under dynamic loading. Several models have been proposed to understand SIC. Furthermore, there are the theories of Gaylord and Lohse [27] proposing models for describing SIC [27–30]. Based on these models, the deformation results in an increase in the distance between the cross-links of the rubber, thereby reducing the entropy of the molecular chains and activating crystallization [31]. The ability to crystallize under tension is an important property of

NR-based rubber as it directly leads to its stiffening [32]. From the perspective of the vulcanization system, respective *CLD*, the crystallization effect decreases with increasing *CLD*, leading to the fact that the optimal crystallization effect occurs in rubber vulcanized by the CV system [33]. It is during CC wear when the tire tread rolls over the axial aperture, and its tip is pushed deep into the rubber matrix, that high local deformation occurs well above the threshold at which crystal formation is induced. This is the main reason why the SIC material is highly resistant to CC wear. The combination of the information on the resistance of the rubber to CC wear due to the SIC effect and the achievement of the optimum effect of crystallization in the CV system makes it clear that it is the rubber with the SIC effect vulcanized by the CV system that is the most suitable candidate for a material resistant to real CC wear. From a chemical point of view, it is clear that vulcanizates containing more polysulfide bonds show a higher rate (SIC) and, therefore, higher CC wear resistance compared to vulcanizates with disulfide and monosulfide bonds [34]. However, it must be clearly understood that for the low load region, where SIC is not induced in rubbers subject to SIC, CC wear is significantly higher than for rubbers not subject to SIC. Thus, the positive effect of SIC as an unrepresented role of the CV system has been demonstrated in previous work by the authors [10]. In this paper, the increased resistance against CC wear of NR-based rubber on SIC has been clearly demonstrated. Moreover, the study definitely confirmed the significantly improved resistance of NR-based rubber against the CC wear cured with the CV system compared to those cured with SEV and EV. However, previous studies were based on varying the *CLD* by varying the A/S ratio by varying the amount of accelerator while keeping the amount of sulfur constant.

Therefore, the present work is focused on the experimental determination of the effect of *CLD* while keeping constant the accelerator-to-sulfur ratio $A/S = 0.2$, which exactly is typical for the CV curing system and thus unambiguously determines the range of network densities within which the optimum mechanical properties and CC wear resistance of the rubber can be achieved. For this ratio, different sulfur quantities of 1/1.5/2.5/4/8/10 and 16 phr (parts per hundred of rubber) were chosen, and the accelerator concentration *N*-tert-butyl-benzothiazole sulfonamide (TBBS) was calculated accordingly respecting

the constant A/S ratio. The studied material was again NR and filled with CB, as in previous published studies.

2. Materials and methods

2.1. Materials

The based material NR (standard Vietnamese rubber with a Mooney viscosity ML(1+4) at 100 °C: 60±5), obtained from Binh Phuoc (Vietnam) under the trade name SVR-CV60-3L, was used as the base for the rubber compounds studied. The filler of amount 58 phr of CB of the type N 220 from Makrochem (Lublin, Poland) has been applied as reinforcing filler, which is characterized due to Iodide absorption ($IA = 121 \pm 6 \text{ g} \cdot \text{kg}^{-1}$) and oil absorption (dibutyl phthalate absorption (DBPA) = $121 \pm 6 \text{ mL} \cdot 100 \text{ g}^{-1}$). The other raw materials contained in the rubber recipe are as follows: antidegradant 2,2,4-trimethyl-1,2-dihydroquinoline (TMQ) from Lanxess (Köln, Germany), antioxidant *N*-(1,3-dimethylbutyl)-*N'*-phenyl-*p*-phenyldiamine (6PPD, Vulkanox 4020) from Lanxess (Köln, Germany), antiozonant Varazon 5998 from Lanxess (Sandton, South Africa), processing aid Tudalen oil 11 from Fraunhofer (München, Germany), activators ZnO from SlovZink a.s. (Košeca, Slovakia), and stearic acid from Setuza a.s. (Ústí nad Labem, Czech Republic), accelerator *N*-tert-butyl-benzothiazole sulfonamid (TBBS) from Duslo a.s. (Šaľa, Slovakia), and curing agent sulfur OT 33 from Estman Chemical Company (Kingsport, TN, USA). Toluene, which was used for the characterization of the rubber swelling to determine the apparent *CLD*, was obtained from Sigma-Aldrich (St. Louis, MO, USA). For the analysis of *CLD* distribution, propan-2-thiol ($\geq 98\%$), dodecan-1-thiol ($\geq 98\%$) and piperidine (99%) were provided by Sigma-Aldrich (St. Louis, MO, USA).

2.2. Preparation of rubber compounds

Seven rubber compounds were prepared while varying the amount of accelerator and sulfur so that the ratio of the accelerator-to-sulfur $A/S = 0.2$ was maintained. The rubber recipe is given in Table 1.

A two-step mixing procedure was employed to prepare all rubber compounds. Both of the steps were made in an internal mixer SYD-2L from Everplast (Taiwan) with a fill factor of 0.75 and a total mixing capacity of 1.25 L. First, the masterbatch was prepared after masticating the virgin rubber for 1 min. Next, the CB together with Tudalen oil 11 were

Table 1. Rubber compound recipe.

Ingredient	Loading [phr]
SVR-CV60-3L	100.0
N 220	58.0
TMQ	2.0
6PPD	2.5
Varazon 5998	2.0
Tudalen oil 11	6.0
ZnO	5.0
Stearic acid	3.0
TBBS	0.2/0.3/0.5/0.8/1.6/2.0/3.2
Sulfur OT33	1.0/1.5/2.5/4.0/8.0/10.0/16.0

added and mixed for another 3.5 min. Additionally, ZnO and stearic acid have been incorporated to the mixture and mixed for another 7 min. The rotor speed was 50 rpm to reaching the temperature of the mixture maximum of 150 °C, whereas the initial temperature was 70 °C. The masterbatch thus prepared was milled over a period of 3 min using a double-roll mill at a rotation speed ratio of 15:12 and sheeted out at rolls of a temperature 70 °C.

The final batch was then prepared by mixing the masterbatch together with sulfur and accelerator for 3 min at a rotor speed of 35 rpm and at an initial temperature of 60 °C followed by adding the complete curing system and mixed until the temperature of the mixture reached 96 °C. The final batch was again milled with a double-roll mill at 60 °C for 3 min. Produced mixtures were stored for 24 h before further analyses.

Curing characteristics were measured according to ASTM D 5289 standard on the premier MDR-moving die rheometer from Alpha Technology (Hudson, OH, USA) at constant temperature of 160 °C. The following parameters have been obtained: minimum torque (M_L), maximum torque (M_H), scorch time (t_{s2}), and optimal curing time (t_{90}). The reversion of curing behavior was calculated and reported in percentage using Equation (1):

$$R_{60} [\%] = \frac{M_H - M_{60}}{M_{60}} \cdot 100 \quad (1)$$

where M_{60} is the torque at 60 min. The reversion was calculated after 60 min of the vulcanization.

Finally, the rubber samples for future tensile and hardness analyses were prepared by compression molding at 160 °C using the hydraulic heating press LabEcon 300 from Fontijne Presses b.v. (Rotterdam, the Netherlands) at constant pressure 200 kPa. The

samples were cured in accordance to optimum curing time t_{90} . On the other hand, the specimens used for the CC wear analysis were molded identically, but at different times $t_{90}+7$ min, with the additional 7 min resulting from the specification of 0.5 min per 1 mm of specimen thickness.

First, the tensile properties, Shore-A hardness, rebound resilience, *CLD* and its distribution were analyzed. The tensile test was performed using the tensile testing machine T10D from Alpha Technology (Hudson, OH, USA) according to ISO 37 standard at the extension rate of 500 mm·min⁻¹ for standard test specimens of the type S2 with 2 mm. Tear strength were measured according to ISO 34–1 using the identical tensile testing machine. The tensile as well as tear strength properties reported in this paper are average values of 5 replicas. The measurement of the Shore-A hardness was performed in accordance with ISO 7619-1 and measured on 5 replicas at time 3 s for each compound. Rebound resilience was determined according to ISO 4662 standard using an identical sample as for Shore-A hardness. Average values of the rebound resilience and their standard deviation were subsequently determined from 6 replicas. Measurements of Shore-A hardness and rebound resilience were performed at laboratory temperature of 23 °C.

The *CLD* calculation is based on the Kraus modified Flory-Rehner formula (Equation (2)) for filled rubber vulcanizate from equilibrium swelling in toluene. Detailed relations for calculating *CLD* are given in a previous publication [10]:

$$v = \frac{-V_{ro} [\ln(1 - V_r) + V_r + \chi V_r^2]}{V_s (\sqrt[3]{V_{ro}^2 V_r} - 0.5V_r)} \quad (2)$$

where V_s is molar volume of toluene, V_r is the volume fraction of the gel in the equilibrium swollen vulcanizate with fillers and V_{ro} the volume fraction of gel in the equilibrium swollen vulcanizate without fillers. χ is the Flory-Huggins polymer-solvent interaction parameter. In the case of NR and toluene as swelling agent $\chi = 0.414$ [17]. Samples for swelling tests were of rectangular shape with the dimensions 20×30×2 mm and the experiment was performed at laboratory temperature of 23 °C.

The distribution of *CLD* according to the type and amount of bonds in the vulcanizate (monosulfide, polysulfide and disulfide) was determined on the basis of two-step thiol-amine reactions [35]. In the

first stage, the partitioning of the polysulfide bonds was achieved by placing the swollen sample in a solution prepared by mixing two solutions of 0.4 M solution of propan-2-thiol in toluene and 0.4 M solution of piperidine in toluene, where M denotes molar concentration in $\text{mol} \cdot \text{dm}^{-3}$. After 24 h, the samples were removed from the solution, decanted, and reinserted in toluene for 24 h for swelling. The samples were weighed after 24 h. In the second step for the disulfide bond cleavage, the process was repeated identically, except that the swollen samples were placed in a 1 M solution of dodecan-1-thiol in piperidine for 24 h of exposure. Finally, the distribution of polysulfide bonds (defined as $v_{\text{polysulfide}}$) was determined from the difference between the total apparent *CLD*, determined by swelling, before (defined as v_{total}) and after (defined as $v_{\text{mono- and disulfide}}$) the treatment and can be expressed as Equation (3):

$$v_{\text{polysulfide}} = v_{\text{total}} - v_{\text{mono- and disulfide}} \quad (3)$$

The distribution of monosulfide bonds was determined after the second step and calculated as Equation (4):

$$v_{\text{disulfidic}} = v_{\text{mono- and disulfidic}} - v_{\text{monosulfidic}} \quad (4)$$

The determination of the rubber resistance to DIN abrasion was performed for 3 replicas per compound in accordance with ISO 4649B, whereby this method is based on the determination of the mass loss relative, Δm_{rel} , as a relative number in %. Δm_{rel} was determined by sliding a rubber test samples over a length of 50 m on a specific abrasive sheet with a

force of 10 N and has been determined as Equation (5):

$$\Delta m_{\text{rel}} [\%] = \frac{m_1 - m_2}{m_1} \cdot 100 \quad (5)$$

where m_1 is the weight of a sample in [g] prior and m_2 after the abrasion. The measurement was performed on cylindrical samples with a diameter of 16 mm and a height of from 6 to 12 mm.

Finally, the CC behavior of all materials represented by the CC damage parameter, P was analyzed at laboratory temperature using the Instrumented cut and chip analyzer (ICCA) from Coesfeld GmbH & Co (Dortmund, Germany) under the following test conditions:

- Rotational speed: 150 rpm,
- normal (impact) forces: 100/150/200 N,
- sliding time: 50 ms,
- impact frequency: 5 Hz,
- total no. of impact cycles: 3000.

Testing device and principles of the testing procedures are described in [36–40] and the complete ICCA analyses have been performed in accordance to the testing protocol described in detail previously in [6, 10].

3. Results and discussion

The curing characteristics are shown in Figure 2, left, and the evaluated curing parameters are listed in Table 2. From Figure 2a, it can be seen that the value of M_H increases with increasing sulfur concentration, with the lowest torque value M_H (9.4 dN·m) given by the mixture with 1 phr sulfur. Obviously, a higher sulfur concentration results in a higher curing

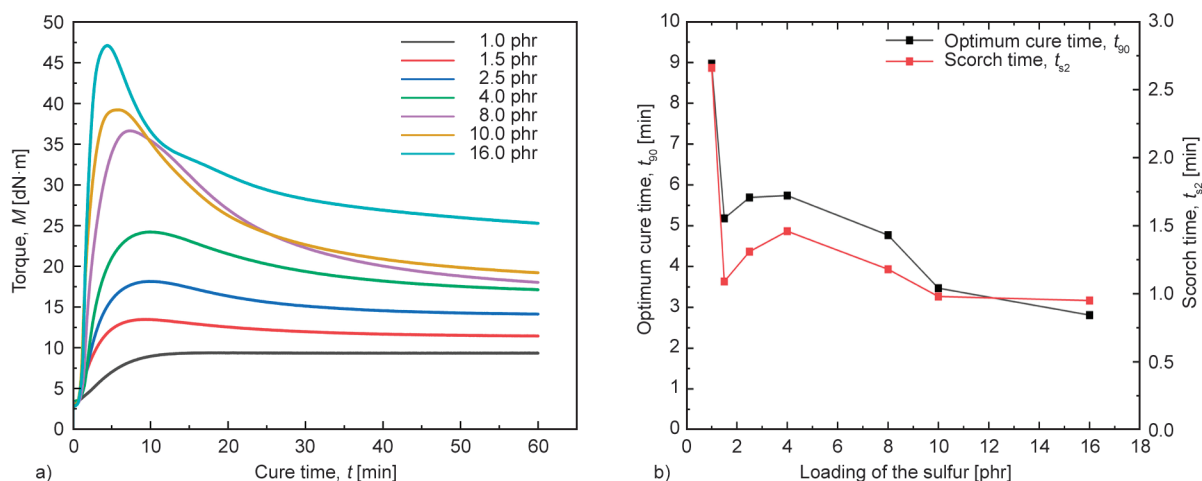


Figure 2. Vulcanization characteristic rubber compound (a) and dependence of curing parameters t_{90} , t_{s2} on the concentration of sulfur (b).

Table 2. Vulcanization of parameters of rubber compounds.

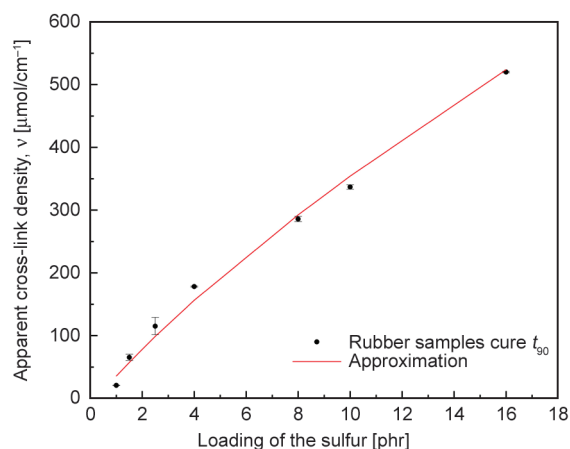
Sulfur content [phr]	M_H [dN·m]	M_L [dN·m]	t_{s2} [min]	t_{90} [min]	Reversion after 60 min of curing [%]
1.0	9.4	3.1	2.7	8.9	0.53
1.5	13.5	2.9	1.1	5.2	16.3
2.5	18.2	3.0	1.3	5.7	22.2
4.0	24.2	3.4	1.5	5.7	29.3
8.0	35.2	2.5	1.2	4.8	49.8
10.0	37.9	2.6	0.9	3.5	51.5
16.0	47.1	2.8	1.0	2.8	46.4

speed. A closer look at these diagrams provides information about the behaviour of the material during curing, which can be expressed by the curing parameters t_{90} and t_{s2} . First of all, a reduction in t_{90} and t_{s2} can be observed for the compounds shown in Figure 2b. The curing parameters t_{90} and t_{s2} initially show a steep decrease with increasing sulfur concentration of 1 to 1.5 phr, followed by a slight increase in the values of t_{90} and t_{s2} up to sulfur concentration of 4 phr, while with subsequently increasing sulfur content the values of both parameters decrease steadily. The mixture with 1 phr sulfur reaches the highest t_{90} value (8.9 min). The lowest t_{90} value (2.8 min) was determined for the compound with the highest sulfur concentration of 16 phr. Table 2 also shows the typical reversal phase values for NR, which were determined for a vulcanization time of 60 min. The results clearly show that the reversion behavior is dependent on the sulfur concentration. No reversion occurs in a compound with a sulfur concentration of 1 phr, whereby the reversion values increase with a further increase in the sulfur concentration up to a sulfur concentration of 10 phr and decrease again at a sulfur concentration of 16 phr. Therefore, it can be said that a local maximum of reversion is reached at 10 phr sulfur.

Figure 3 shows the dependence of CLD on sulfur concentration for the material cured with respect to t_{90} . In order to describe the relationship between sulfur concentration and CLD by a continuous analytical function with maximum accuracy, a specific function (Equation (6)) with a maximum coefficient of determination, R^2 was found in accordance with the method used in [41]:

$$CLD = (a \cdot \sqrt[3]{S} + b)^2 \quad (6)$$

where S is the concentration of the sulfur, and a and b are the numerically determined coefficients. A

**Figure 3.** Dependence of the CLD on sulfur concentration.**Table 3.** CLD related to sulfur concentration.

Sulfur concentration [phr]	CLD, v [$\mu\text{mol}\cdot\text{cm}^{-3}$]
1.0	35
1.5	57
2.5	99
4.0	156
8.0	292
10.0	354
16.0	52

value of 0.01134 was calculated for a , and -0.00517 for b . Table 3 summarizes the CLD values corresponding to the sulfur concentration with the numerical CLD values determined from the approximation function (Equation (6)). The approximation is further used in this work to assign mechanical properties to the CLD values analyzed in this study.

The percentage distribution of CLD as a function of sulfur concentration is presented in Table 4, and the distribution of polysulfide, disulfide, and monosulfide bonds can be observed. For samples with low CLD , corresponding to sulfur concentrations of 1 and 1.5 phr, only the content of polysulfide bonds could be determined, whereas materials with such low CLD contain only a minimum of disulfide and monosulfide bonds, which could not be determined due to the low CLD . Moreover, a material with such a low CLD broke down upon breaking the polysulfide bonds, where such samples are marked as unanalyzable in Table 4. It can be determined that approximately 90% of these CV curing systems are just polysulfide bonds. Just as mentioned above, the presence of the maximum amount of polysulfide bonds is crucial for a higher rate of SIC formation [34] and a significant reduction in CC wear. It was then further determined that the amount of monosulfide bonds

Table 4. Distribution of the *CLD*.

Sulfur content [phr]	Polysulfide bonds [%]	Disulfide bonds [%]	Monosulfide bonds [%]
1.0	Unanalyzable	Unanalyzable	Unanalyzable
1.5	88.2	Unanalyzable	Unanalyzable
2.5	90.1	4.5	5.4
4.0	87.8	9.9	2.3
8.0	90.5	8.3	1.2
10.0	90.0	9.3	0.7
16.0	92.7	6.8	0.5

decreases with increasing sulfur concentration, with the monosulfide bond content determined to be 5.4% for samples with 2.5 phr sulfur and with further increases in sulfur concentration of 10 phr (0.7%) and 16 phr (0.5%) monosulfide bonds can be observed. The tensile properties, namely the stress and elongation at break, as a function of the *CLD*, are shown in Figure 4a. The stress at break for low *CLD* values increases to a value of $160 \mu\text{mol}\cdot\text{cm}^{-3}$, where its value reaches 26 MPa, and then steadily decreases with further increase in *CLD*. It should be noted that stress at break values higher than 20 MPa, considered standard high values, are obtained for all the *CLDs* analyzed except for the lowest value of $35 \mu\text{mol}\cdot\text{cm}^{-3}$. On the other hand, the elongation at break steadily decreases with increasing *CLD*. Figure 4b, illustrates the dependence of Shore-A hardness and rebound resilience on *CLD*, and the waveforms for both dependencies are almost identical and show a growth with increasing *CLD*. The steepest increase is then observed for hardness up to a value of $300 \mu\text{mol}\cdot\text{cm}^{-3}$ and for rebound resilience up to a value of $160 \mu\text{mol}\cdot\text{cm}^{-3}$, whereas for other values of *CLD*, the increase is only gradual.

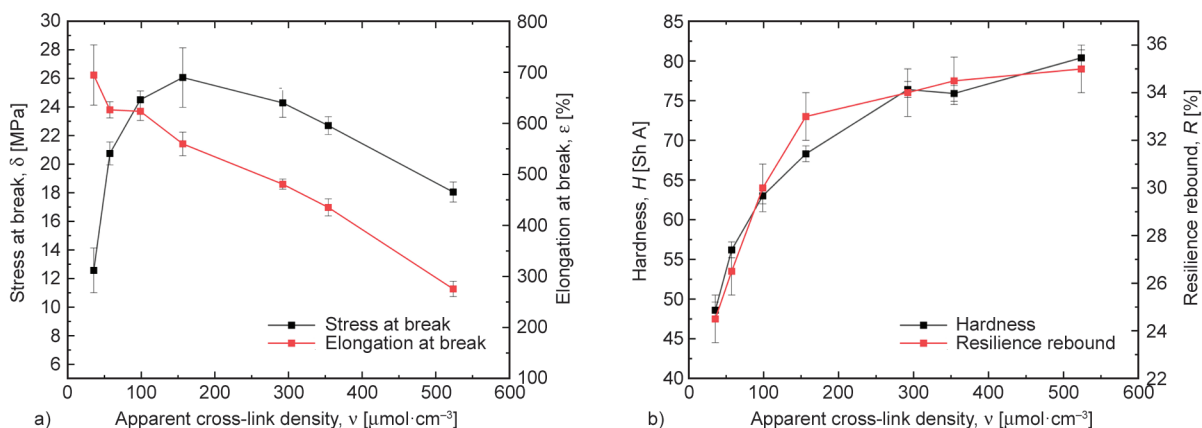


Figure 4. Tensile properties (a), Shore-A hardness and rebound resilience (b) as a function of *CLD*.

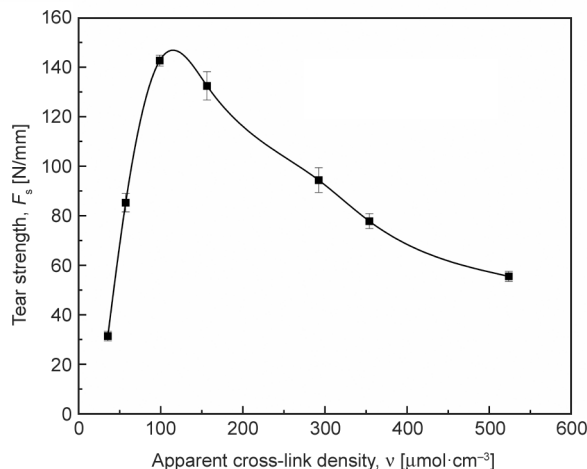


Figure 5. Tear strength in dependence on *CLD*.

The tear strength dependence for the type of angular test specimen is shown in Figure 5. It can be seen that a significant increase in tear strength occurs in the region of *CLD* approximately from 35 to $100 \mu\text{mol}\cdot\text{cm}^{-3}$. For the $CLD = 100 \mu\text{mol}\cdot\text{cm}^{-3}$, the maximum tear strength ($140 \text{ N}\cdot\text{mm}^{-1}$) can be observed. It is evident that from this value onwards there is a decrease in tear strength. It can, therefore, be concluded that the maximum resistance to crack growth is provided by this system around $CLD = 100 \mu\text{mol}\cdot\text{cm}^{-3}$, only.

Figure 6 shows the dependence of DIN abrasion represented by the mass loss relative Δm_{rel} on *CLD*. The material with the lowest $CLD = 35 \mu\text{mol}\cdot\text{cm}^{-3}$ shows the highest value of relative weight loss, up to 6.6%. However, a slight increase in *CLD* to about $60 \mu\text{mol}\cdot\text{cm}^{-3}$ shows a significant decrease in mass loss relative to a value of about 2.6%, which remains almost constant up to $160 \mu\text{mol}\cdot\text{cm}^{-3}$. With a further increase in *CLD*, the relative weight loss value

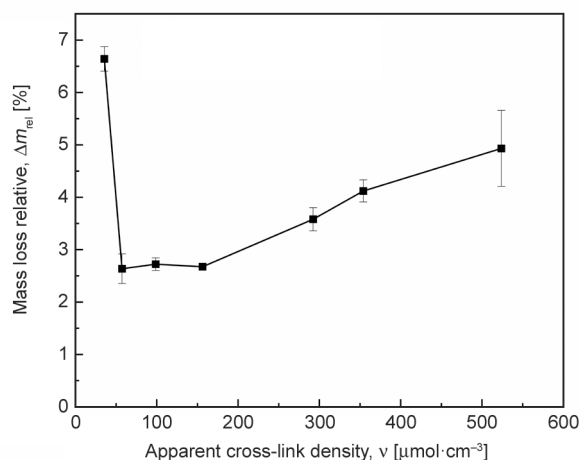


Figure 6. Mass loss for DIN abrasion in dependence on *CLD*.

increases steadily again, but even for the highest value of $CLD = 530 \mu\text{mol}\cdot\text{cm}^{-3}$, it is still significantly lower, 4.9 %, compared to the highest measured value of $CLD = 35 \mu\text{mol}\cdot\text{cm}^{-3}$. Thus, this relationship clearly shows that materials with *CLD* in the range of 60 to 160 cm^{-3} show the highest DIN abrasion resistance.

Finally, the dependence of the CC wear represented by the CC damage parameter, P , on the *CLD* will be discussed, where this dependence is plotted in Figure 7 for different loads. Figure 7a shows the dependence for the whole range of *CLD*, whereas Figure 7b only details the dependence from the lowest *CLD* value up to $150 \mu\text{mol}\cdot\text{cm}^{-3}$. For a clear understanding of CC behavior, each curve must be discussed individually. The dependence of CC damage parameter, P on *CLD* for the lowest load of 100 N shows a slight increase from the lowest *CLD* value

at first, but immediately after reaching $60 \mu\text{mol}\cdot\text{cm}^{-3}$ CC damage parameter, P starts to decrease again up to $CLD = 130 \mu\text{mol}\cdot\text{cm}^{-3}$. With a further increase in *CLD*, the CC damage parameter, P , increases significantly up to about $400 \mu\text{mol}\cdot\text{cm}^{-3}$, when for the highest *CLD*, it decreases again slightly. In contrast, the CC damage parameter, P for the intermediate load of 150 N increases with increasing *CLD* value over the entire *CLD* region. Here, however, it is necessary to concentrate on the detailed *CLD* region only up to $150 \mu\text{mol}\cdot\text{cm}^{-3}$, in which up to a value of about $70 \mu\text{mol}\cdot\text{cm}^{-3}$, the CC damage parameter, P values for a medium load of 150 N are significantly lower than for a loading force of 100 N. After this value is exceeded, the CC damage parameter, P , for 150 N, is then significantly higher than for lower force. The CC damage parameter, P , for the highest load of 200 N, is slightly higher than for the two remaining loads at the lowest *CLD* but decreases with a further increase to a value of $CLD = 60 \mu\text{mol}\cdot\text{cm}^{-3}$. With a further increase in *CLD*, the CC damage parameter, P value, increases steadily, but still, in the range of about 40 to $90 \mu\text{mol}\cdot\text{cm}^{-3}$, the damage parameter, P value, is the lowest of all loads applied. With a further increase in *CLD*, the CC damage parameter, P value for a 200 N load, is already higher than for a 100 N load but still lower than for a 150 N load up to a value of $CLD = 150 \mu\text{mol}\cdot\text{cm}^{-3}$. The effect of SIC is evident in the curves for loads of 150 and 200 N, wherein the *CLD* region from 50 to $90 \mu\text{mol}\cdot\text{cm}^{-3}$, the minimum values of the CC damage parameter, and the P parameter are just for the highest loads without the sharp slope that occurs with further increase in *CLD*. Thus, in this region,

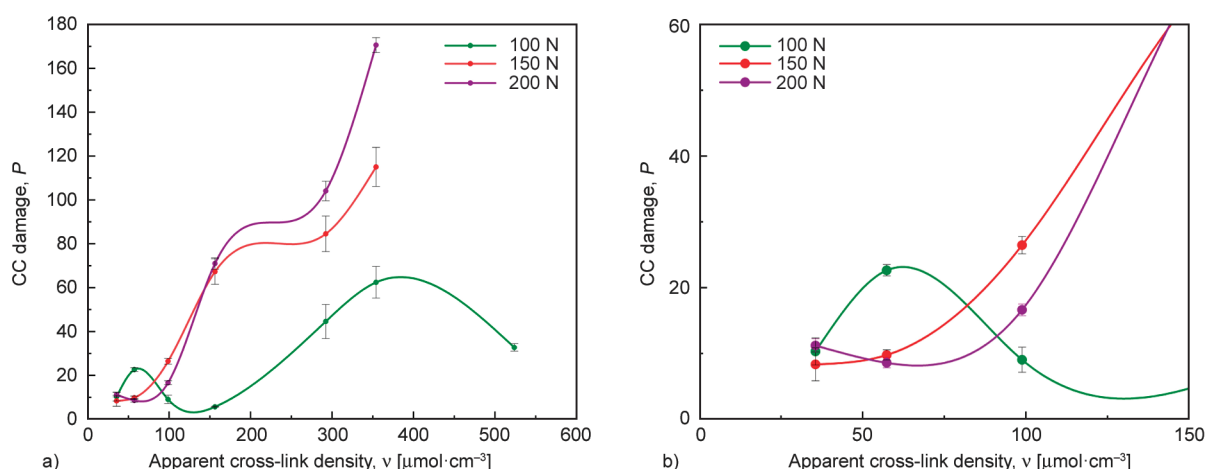


Figure 7. Dependence of CC damage parameter, P on *CLD* (a) and detailed view up to $160 \mu\text{mol}\cdot\text{cm}^{-3}$ (b).


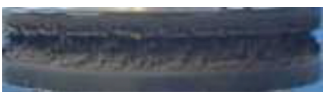
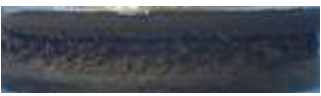



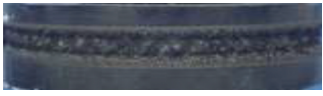
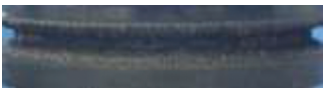



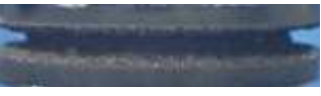
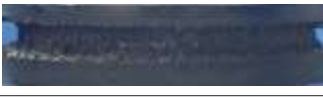
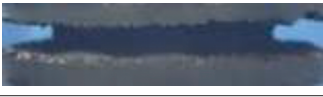







crystals are formed at such intense loads, which strengthen the rubber matrix, and the rubber becomes more resistant to CC wear.

Table 5 shows photographs of CC wear on the surfaces of the samples after the CC analysis has been completed. The structure of the CC worn surface corresponds to the CC damage parameter, P values in the plots in Figure 7, where with lower CC damage parameter, P values, the structure of the CC wear on the surface is also lower and vice versa. It is particularly interesting to observe the surface for $CLD = 57 \mu\text{mol}\cdot\text{cm}^{-3}$, for which it is clearly seen that indeed, the lowest CC wear structure is exhibited by the sample loaded with 200 N followed by the surface of the sample loaded with 150 N and the most significant CC wear structure is exhibited by the sample loaded with the lowest force of 100 N. The samples with $CLD = 99 \mu\text{mol}\cdot\text{cm}^{-3}$ already shows a significantly higher CC wear structure for the samples loaded with 150 and 200 N compared to the load of 100 N. This trend, where the samples loaded with the lowest force show the lowest CC wear structure compared to the samples loaded with both higher loads, remains consistent with increasing CLD .

4. Conclusions

This work extends previous research [10] by the authors that aimed to describe the effects of apparent CLD on the wear of NR in order to highlight the positive effect of CV. Therefore, the present work focuses on the experimental determination of the influence of CLD at a constant accelerator-to-sulfur ratio $A/S = 0.2$. All investigated compounds, $CLDs$ ranging from 35 to $524 \mu\text{mol}\cdot\text{cm}^{-3}$ were determined. Initially, standard analyses of tensile strength, Shore-A hardness, rebound resilience, and DIN abrasion were performed to determine their dependencies on CLD . With increasing CLD , an increase in Shore-A hardness and rebound resilience and a decrease in elongation at break were observed. The stress at break increases with increasing CLD up to a value of about $160 \mu\text{mol}\cdot\text{cm}^{-3}$, then the trend reversed. The steady-state abrasion was determined using the DIN Abrader device, with the values for mass loss decreasing with increasing CLD to around $60 \mu\text{mol}\cdot\text{cm}^{-3}$ and remaining more or less constant up to $160 \mu\text{mol}\cdot\text{cm}^{-3}$ before increasing again. In terms of typical rubber mechanical properties, the compounds reached optimum values in the CLD range of 60 to $160 \mu\text{mol}\cdot\text{cm}^{-3}$.

Table 5. Photograph of worn rubber surface after CC analysis at 1:1.32 scale.

Sulfur content [phr]	CLD, v [$\mu\text{mol}\cdot\text{cm}^{-3}$]	Normal force, F_N		
		100 [N]	150 [N]	200 [N]
1.0	35			
1.5	57			
2.5	99			
4.0	156			
8.0	292			
10.0	254			
16.0	524			

ICCA was used to determine the resistance of the rubber to CC wear as a function of *CLD*.

In contrast to the optimum *CLD* range in terms of mechanical properties, the highest resistance of our compounds to CC wear was found in the range from 35 to 100 $\mu\text{mol}\cdot\text{cm}^{-3}$. However, the positive effect of SIC was only pronounced in the range from 35 to about 80 $\mu\text{mol}\cdot\text{cm}^{-3}$, which slightly reduces the effective *CLD* range.

Thus, for practical applications, this work narrows down the *CLD* range for the CV curing system, in which the rubber achieves both optimal mechanical properties and resistance to CC wear, to around 60–80 $\mu\text{mol}\cdot\text{cm}^{-3}$. This work is the first to present data that defines the effective *CLD* range in relation to the cross-linking system in order to achieve optimal resistance to CC wear in addition to the rubber's physical properties.

The investigations presented here can be seen as a concept for solving the known conflicts of technical objectives in the so-called magic polygon of tire development on the material side.

Acknowledgements

This work was supported by the Ministry of Education, Youth and Sports of the Czech Republic-DKRVO (RP_CPS_2024_28_006). G. Heinrich acknowledges the DFG (Deutsche Forschungsgemeinschaft) research training group 'Interactive Fiber-Rubber Composites' Project 380321452/GRK2430.

References

- [1] Scherbakov M., Gurvich M. R.: A method of wear characterization under cut, chip and chunk conditions. *Journal of Elastomers and Plastics*, **35**, 73–84 (2003).
<https://doi.org/10.1177/009524403031097>
- [2] Ma S., Huang G., Obaia K., Moon S. W., Liu W. V.: A novel phenomenological model for predicting hysteresis loss of rubber compounds obtained from ultra-large off-the-road tires. *Proceedings of the Institution of Mechanical Engineers Part D: Journal of Automobile Engineering*, **237**, 207–223 (2023)
<https://doi.org/10.1177/09544070211072494>
- [3] Manivasakam N.: Rubber industry. in 'Industrial effluents: Origin, characteristics, effects, analysis and treatment' (ed.: Manivasakam N.) Chemical Publishing, Gloucester, 1–2 (2016).
- [4] Chandrasekaran C.: Anticorrosive rubber lining: A practical guide for plastics engineer. William Andrew, Norwich (2017).
- [5] Boden J., Bowen C. R., Buchard A., Davidson M. G., Norris C.: Understanding the effects of cross-linking density on the self-healing performance of epoxidized natural rubber and natural rubber. *ACS Omega*, **7**, 15098–15105 (2022).
<https://doi.org/10.1021/acsomega.2c00971>
- [6] Stoček R., Heinrich G., Kipscholl R., Kratina O.: Cut & chip wear of rubbers in a range from low up to high severity conditions. *Applied Surface Science Advances*, **6**, 100152 (2021).
<https://doi.org/10.1016/j.apsadv.2021.100152>
- [7] Robertson C. G., Stoček R., Kipscholl C., Mars W. V.: Characterizing the intrinsic strength (fatigue threshold) of natural rubber/butadiene rubber blends. *Tire Science and Technology*, **47**, 292–307 (2019).
<https://doi.org/10.2346/tire.19.170168>
- [8] Robertson C. G., Stoček R., Mars W. V.: The fatigue threshold of rubber and its characterization using the cutting method. in 'Fatigue crack growth in rubber materials' (eds.: Heinrich G., Kipscholl R., Stoček R.) Springer, Cham, 57–83 (2020).
https://doi.org/10.1007/12_2020_71
- [9] Fisher H. L.: Vulcanization of rubber. *Industrial and Engineering Chemistry*, **31**, 1381–1389 (1939).
<https://doi.org/10.1021/ie50359a015>
- [10] Pöschl M., Stoček R., Zádrapa P.: The effect of apparent cross-link density on cut and chip wear in natural rubber. in 'Degradation of elastomers in practice, experiments and modelling' (eds.: Heinrich G., Kipscholl R., Stoček R.) Springer, Cham, 273–291 (2022).
https://doi.org/10.1007/12_2022_129
- [11] Coran A. Y.: Vulcanization. in 'The science and technology of rubber' (eds.: Mark J. E., Erman B., Roland M.) Academic Press, Waltham, 337–381 (2013).
<https://doi.org/10.1016/B978-0-12-394584-6.00007-8>
- [12] Hamed G. R.: Materials and compounds. in 'Engineering with rubber' (ed.: Gent A. N.) Hanser, Cincinnati, 11–36 (2012).
<https://doi.org/10.3139/9783446428713.002>
- [13] Pöschl M., Sathi S. G., Stoček R.: Tuning the curing efficiency of conventional accelerated sulfur system for tailoring the properties of natural rubber/bromobutyl rubber blends. *Materials*, **15**, 8466 (2022).
<https://doi.org/10.3390/ma15238466>
- [14] Pöschl M., Sathi S. G., Stoček R., Kratina O.: Rheometer evidences for the *co*-curing effect of a bismaleimide in conjunction with the accelerated sulfur on natural rubber/chloroprene rubber blends. *Polymers*, **13**, 1510 (2021).
<https://doi.org/10.3390/polym13091510>
- [15] Joseph A. M., George B., Madhusoodanan K. N., Alex R.: Current status of sulphur vulcanization and devulcanization chemistry: Process of vulcanization. *Rubber Science*, **28**, 82–121 (2015).

- [16] Kruželák J., Sýkora R., Hudec I.: Vulcanization of rubber compounds with peroxide curing systems. *Rubber Chemistry and Technology*, **90**, 60–88 (2017).
<https://doi.org/10.5254/rct.16.83758>
- [17] Kim D. Y., Park J. W., Lee D. Y., Seo K. H.: Correlation between the crosslink characteristics and mechanical properties of natural rubber compound *via* accelerators and reinforcement. *Polymers*, **12**, 2020 (2020).
<https://doi.org/10.3390/polym12092020>
- [18] Kruželák J., Kvasničáková A., Hložeková K., Dosudil R., Gořalík M., Hudec I.: Experimental investigation of absorption shielding efficiency of rubber composites. *Polymer Bulletin*, **80**, 13051–13068 (2023).
<https://doi.org/10.1007/s00289-023-04684-x>
- [19] Sathi S. G., Stoček R., Kratina O.: Reversion free high-temperature vulcanization of cis-polybutadiene rubber with the accelerated-sulfur system. *Express Polymer Letters*, **14**, 823–837 (2020).
<https://doi.org/10.3144/expresspolymlett.2020.68>
- [20] Bornstein D., Pazur R. J.: The sulfur reversion process in natural rubber in terms of crosslink density and crosslink density distribution. *Polymer Testing*, **88**, 106524 (2020).
<https://doi.org/10.1016/j.polymertesting.2020.106524>
- [21] Fan R. L., Zhang Y., Li F., Zhang Y. X., Sun K., Fan Y. Z.: Effect of high-temperature curing on the crosslink structures and dynamic mechanical properties of gum and N330-filled natural rubber vulcanizates. *Polymer Testing*, **20**, 925–936 (2001).
[https://doi.org/10.1016/S0142-9418\(01\)00035-6](https://doi.org/10.1016/S0142-9418(01)00035-6)
- [22] Zhao F., Bi W., Zhao S.: Influence of crosslink density on mechanical properties of natural rubber vulcanizates. *Journal of Macromolecular Science Part B: Physics*, **50**, 1460–1469 (2011).
<https://doi.org/10.1080/00222348.2010.507453>
- [23] Dong W., Tang R.: Preparation of NR/SBR blends and their biopolymeric derivatives for water treatment usage *via* different sulfur curing systems. *Polymer Science*, **9**, 1–11 (2020).
<https://doi.org/10.26434/chemrxiv.9971285.v9>
- [24] Mansilla M. A., Marzocca A. J., Macchi C., Samoza A.: Natural rubber/styrene-butadiene rubber blends prepared by solution mixing: Influence of vulcanization temperature using a SEMI-EV sulfur curing system on the microstructural properties. *Polymer Testing*, **63**, 150–157 (2017).
<https://doi.org/10.1016/j.polymertesting.2017.07.025>
- [25] Nie Y., Gu Z., Wei Y., Hao T., Zhou Z.: Features of strain-induced crystallization of natural rubber revealed by experiments and simulations. *Polymer Journal*, **49**, 309–317 (2017).
<https://doi.org/10.1038/pj.2016.114>
- [26] Trabelsi S., Albouy P.-A., Rault J.: Effective local deformation in stretched filled rubber. *Macromolecules*, **36**, 9093–9099 (2003).
<https://doi.org/10.1021/ma0303566>
- [27] Gaylord R. J., Lohse D. J.: Morphological changes during oriented polymer crystallization. *Polymer Engineering and Science*, **16**, 163–167 (1979).
<https://doi.org/10.1002/pen.760160308>
- [28] Candau N., Laghmach R., Chazeau L., Chenal J.-M., Gauthier C., Biben T., Munch E.: Strain-induced crystallization of natural rubber and cross-link densities heterogeneities. *Macromolecules*, **47**, 5815–5824 (2014).
<https://doi.org/10.1021/ma5006843>
- [29] Sotta P., Albouy P. A.: Strain-induced crystallization in natural rubber: Flory’s theory revisited. *Macromolecules*, **53**, 3097–3109 (2020).
<https://doi.org/10.1021/acs.macromol.0c00515>
- [30] Candau N., Chazeau L., Chenal J.-M., Gauthier C., Ferreira J., Munch E., Rochas C.: Characteristic time of strain induced crystallization of crosslinked natural rubber. *Polymer*, **53**, 2540–2543 (2012).
<https://doi.org/10.1016/j.polymer.2012.04.027>
- [31] Boutaous M., Zinet M., Boyard N., Bailleul J.-L.: Phase change kinetics within process conditions and coupling with heat transfer. in ‘Heat transfer in polymer composite materials: Forming processes’ (ed.: Boyard N.) Wiley, Hoboken, 138–140 (2016).
<https://doi.org/10.1002/9781119116288.ch4>
- [32] González L., Rodríguez A., Valentín J. L., Marcos-Fernández A., Posadas P.: Conventional and efficient crosslinking of natural rubber: Effect of heterogeneities on the physical properties. *KGK-Kautschuk Gummi Kunststoffe*, **58**, 638–643 (2005).
- [33] Chenal J.-M., Gauthier C., Chazeau L., Guy L., Bomal Y.: Parameters governing strain induced crystallization in filled natural rubber. *Polymer*, **48**, 6893–6901 (2007).
<https://doi.org/10.1016/j.polymer.2007.09.023>
- [34] Lin F., Jia W., Zhong L., Liu F., Zhang H., Wang B., Song Y.: Effect of main chain modification during reversion on strain-induced crystallization of polyisoprene rubbers. *Polymer Engineering and Science*, **62**, 1710–1719 (2022).
<https://doi.org/10.1002/pen.25958>
- [35] Saiwari S., Dierkes W. K., Noordermeer J. W. M.: Recycling of individual waste rubbers. in ‘Rubber recycling: Challenges and developments’ (eds.: Kim J. K., Saha P., Thomas S., Haponiuk J. T., Aswathi M. K.) Royal Society of Chemistry, London, 186–232 (2019).
<https://doi.org/10.1039/9781788013482-00186>
- [36] Stoček R., Mars W. V., Robertson C. G., Kipscholl R.: Characterizing rubber’s resistance against chip and cut behavior. *Rubber World*, **257**, 38–40 (2018).
- [37] Stoček R., Mars W. V., Kipscholl R., Robertson C. G.: Characterisation of cut and chip behaviour for NR, SBR and BR compounds with an instrumented laboratory device. *Plastics, Rubber and Composites*, **48**, 14–23 (2019).
<https://doi.org/10.1080/14658011.2018.1468161>

- [38] Stoček R., Heinrich G., Schulze A., Wunde M., Klüppel M., Vatterott C., Tschimmel J., Lacayo-Pineda J., Kipscholl R.: Chip and cut wear of truck tire treads: Comparison between laboratory and real tire testing. *KGK-Kautschuk Gummi Kunststoffe*, **73**, 51–55 (2020).
- [39] Stoček R., Ghosh P., Machů A., Chanda J., Mukhopadhyay R.: Fatigue crack growth vs. chip and cut wear of NR and NR/SBR blend-based rubber compounds. in 'Fatigue crack growth in rubber materials: Experiments and modelling' (eds.: Heinrich G., Kipscholl R., Stoček R.) Springer, Cham, 225–244 (2020). https://doi.org/10.1007/12_2020_67
- [40] Kipscholl R., Stoček R.: Degradation of tires during intended usage. in 'Degradation of elastomers in practice, experiments and modeling' (eds.: Heinrich G., Kipscholl R., Stoček R.) Springer, Cham, 185–207 (2022). https://doi.org/10.1007/12_2022_132
- [41] Stoček R.: Some revisions of fatigue crack growth characteristics of rubber. in 'Fatigue crack growth in rubber materials: Experiments and modelling' (eds.: Heinrich G., Kipscholl R., Stoček R.) Springer, Cham, 1–18 (2021) https://doi.org/10.1007/12_2020_72